Biosensors and Bioelectronics 49 (2013) 176–183

Contents lists available at SciVerse ScienceDirect

Biosensors and Bioelectronics

journal homepage: www.elsevier.com/locate/bios

Label-free analysis of prostate acini-like 3D structures by lensfree imaging

Monika E. Dolega [a,b,c], Cédric Allier [d], Srikanth Vinjimore Kesavan [d], Sophie Gerbaud [a,b,c], Frédérique Kermarrec [a,b,c], Pierre Marcoux [d], Jean-Marc Dinten [d], Xavier Gidrol [a,b,c], Nathalie Picollet-D'Hahan [a,b,c,*]

[a] CEA, DSV iRTSV, Biologie à Grande Echelle, Biomics, 17 rue des Martyrs, F-38054 Grenoble, France
[b] INSERM, U1038, F-38054 Grenoble, France
[c] Université Joseph Fourier-Grenoble I, U1038, F-38041 Grenoble, France
[d] CEA, LETI, MINATEC, 17 rue des Martyrs, F-38054 Grenoble, France

ARTICLE INFO

Article history:
Received 14 March 2013
Received in revised form
29 April 2013
Accepted 2 May 2013
Available online 21 May 2013

Keywords:
Lensfree imaging
Prostate
Acini
3D culture
Morphogenesis
Cancer

ABSTRACT

We present a lensfree imaging method to analyze polarity in RWPE1 prostate epithelial cells that form polarized acini with lumen under standard tridimensional (3D) culture conditions. The first event in epithelial carcinogenesis is loss of polarity, followed by uncontrolled proliferation leading to metastasis. We demonstrate that it is possible to use optical signatures to discriminate 3D objects with distinct polarities in a large field of view. The three metrics we present here are designed as image processing tools to discriminate acini from spheroids without any 3D reconstruction. To demonstrate that our lensfree imaging platform may be used to study the 3D organization of epithelial cells, we analyzed and quantified the modulation of dynamic processes, e.g., the polarity of acini and the merging of polarized structures, upon transforming growth factor beta-1 (TGF beta-1) addition to the culture media. Hence, coupling lensfree microscopy with 3D cell culture provides an innovative tool to study epithelial tissue morphogenesis in a large field of view and to elucidate the regulation of growth, morphogenesis and differentiation in normal and cancerous human prostate cells. Moreover, such biosensor would be a powerful tool to follow cancer progression and to evaluate anti-cancer drugs.

1. Introduction

For many decades, cell biology experiments have been based on two dimensional (2D) cell cultures on rigid plastic substrates. Unfortunately, such culture conditions poorly reflect the reality of the cell microenvironment, which is composed of a fibrous network of proteins from the extracellular matrix (ECM) and neighboring cells in a tridimensional (3D) configuration. Cell culture in 3D offers a more realistic model of the in vivo microenvironment that favors polarized cell–cell and cell–ECM interactions (Pampaloni et al., 2007). Therefore, 3D cell culture is becoming routine in cell biology laboratories, and systems enabling the more complex reconstruction of tissues have been proposed (Mailleux et al., 2008; Pearson et al., 2009; Bryant and Mostov, 2008; O'Brien et al., 2002; Zegers et al., 2003). In this paper, we focus on the study of acini, which are the basic 3D structures constituting a secretory epithelium. The integrity of fully differentiated acini is determined by their apical and basal polarities, which are both characterized by specific cell–basement membrane contacts, intercellular junctions and luminal apoptotic cells (Debnath and Brugge, 2005). The maintenance of this polarity is critical for the structure and function of epithelial cells. The mechanisms controlling epithelial polarity and lumen formation are poorly understood (Pearson et al., 2009). Moreover, the disruption of apical polarity and the progressive transformation of acini into spheroids are key events in tumor progression. Therefore, the analysis of cell polarity is critical to assess epithelial development, integrity and homeostasis and to study the pathogenesis of epithelial tumors. To properly analyze polarity, in vitro 3D culture systems are necessary and are of increasing interest for cancer research because they recapitulate in vitro the alteration of the tissue architecture that precedes tumor development. Moreover, tissue architecture and the ECM influence the responses of tumor cells to signals from the microenvironment provided in a 3D context.

The imaging of 3D polarized structures in culture is not developing as fast as the 3D culture systems themselves. Immunofluorescence imaging of apical and basal polarity markers in fixed cells is the classical approach to study epithelial tissue phenotypes (Lee et al., 2007). It provides a way to follow the loss of apical

* Corresponding author at: CEA, DSV iRTSV, Biologie à Grande Echelle, Biomics, 17 rue des Martyrs, F-38054 Grenoble, France. Tel.: +33 4 38 78 67 78; fax: +33 4 38 78 59 17.
E-mail address: nathalie.picollet-dhahan@cea.fr (N. Picollet-D'Hahan).

0956-5663/$ - see front matter © 2013 Elsevier B.V. All rights reserved.
http://dx.doi.org/10.1016/j.bios.2013.05.001

polarity that is often described by the redistribution of tight junction proteins away from apical sites and by the filling of the lumen by disorganized cells, indicating that acini are transforming into spheroids (Hebner et al., 2008). However, the immunostaining approach presents some limitations (Yue et al., 2012), one being that it remains expensive because it is time-consuming and costly. In addition, data acquisition from living cells requires the use of transfection to induce the stable fluorescent expression of particular proteins, and the side effects on cellular function have to be considered (Baum et al., 2003). For clinical purposes, those traditional methods are not suited for the rapid and high-throughput counting/imaging of 3D cultures and the high-throughput evaluation of drugs that would cause high-throughput increase of the acinar forming ability of the cells while decreasing their invasiveness.

To overcome the above-mentioned limitations, a new imaging methodology to fully exploit the benefits of 3D cultures is needed. A direct imaging technique would (i) allow the observation of living cells, (ii) not require any staining, (iii) be time-efficient and (iv) enable high-throughput analysis and hence provide satisfactory statistical data.

As reviewed recently in Greenbaum et al. (2012), there is great potential for imaging without lenses, i.e., on-chip cell imaging and lensfree holographic microscopy. The resolution of these techniques is approximately 1 μm and can hardly compete with microscopy, but they offer several other advantages: the field of view (FOV) can cover up to several cm^2, the equipment is mostly compact in size; there is a wide range of readouts ranging from 1 nm to 1 mm; and they are easy to use. The e-Petri dish (Zheng et al., 2011), an on-chip cell imaging platform based on shadow imaging, challenges the superiority of video microscopy for applications such as cell migration assays. It allows continuous monitoring over a large field of view (24 mm^2), enabling the live imaging of thousands of cells simultaneously, but it remains limited to 2D cell culture. Moreover, the system requires a specific cell culture chamber and the customization and skillful integration of a sensor; 3D cell culture imaging with such a device has not yet been demonstrated. The second method, lensfree holographic microscopy, is very efficient for the detection of biological objects over very large FOVs (>20 mm^2) (Bishara et al., 2011; Mudanyali et al., 2011; Allier et al., 2010). Recently, it has been used to detect viruses (Mudanyali et al., 2013), to perform high-throughput 3D tracking of human sperm (Su et al., 2012) and to image microvessels from endothelial cells (Weidling et al., 2012). Little has been done to use lensfree holographic microscopy for monitoring cell culture (Moscelli et al., 2011), although it offers great promise for observing 3D cell cultures and even reconstructed tissues (Weidling et al., 2012; Isikman et al., 2011). Lensfree imaging could be used in difficult cellular assays for the quantification and analysis of complex cellular responses to address fundamental questions in developmental biology and to evaluate the effects of drugs in a physiological context.

Here, we use lensfree imaging to observe 3D structures from epithelial cells. We demonstrate that it is possible to use distinct optical signatures to quickly discriminate 3D objects of different polarities in a large field of view. Each object may exhibit either a well-ordered architecture (acinus) or a disrupted 3D structure with filled luminal space (spheroid). The three metrics we present here, i.e., gray level, Zernike features and the reconstructed holographic amplitude, are designed as image processing tools to discriminate acini from spheroids without 3D reconstruction. To illustrate the capabilities of our lensfree imaging platform, we showed how the 3D microenvironment influences 3D epithelial cell morphology and the merging of a population of cells. More specifically, we studied the effects of transforming growth factor beta-1 on acini size, lumen presence and acini merging, supported by strong statistical data.

This imaging system could be used extensively for studying cell–cell and cell–environment interactions by modulating the biochemical and mechanical stimuli within the ECM. We believe that this imaging system will be a powerful method for the large field analysis of multiple soluble effects, including fundamental and pharmacological research in carcinogenesis.

2. Materials and methods

2.1. Cell lines

RWPE1 and WPE1-NB26 cells were used in this study as models for normal and malignant epithelial acinar morphologies, showing two distinct and well-characterized phenotypes in 3D. The RWPE-1 cell line was obtained from ATCC (CRL-11609). This cell line was derived from non-neoplastic human prostate epithelial cells by immortalization with human papillomavirus (22). The WPE1-NB26 cells were derived from RWPE-1 cells by exposure to a direct-acting carcinogen, N-methyl-N-nitrosourea, and were purchased from ATCC (CRL-2852). The RWPE1 cells mimic normal prostate epithelial cell behavior as characterized by a well-established polarized morphology, whereas the WPE1-NB26 cells represent tumorigenic cells at a highly invasive stage of neoplastic transformation with the loss of acinar morphogenesis.

2.2. Cell culture (2D and 3D) and staining

RWPE1 and WPE1-NB26 cells were both maintained in KSFM (Life Technologies, Carlsbad, CA, ref. 17005-075) supplemented with 5 ng/mL epidermal growth factor (EGF) and 50 μg/mL bovine pituitary extract. The cells were maintained in culture until approximately 70% confluency. For passaging, cells were washed with Dulbecco's Ca^{2+}/Mg-free PBS (D-PBS, Life Technologies, ref. 14190) and incubated with 1 mL trypsin–EDTA (Lonza, Basel, CH, ref. CC-5012, 0.25 mg/mL) for approximately 7 min. The trypsin was neutralized with 2 ml trypsin neutralizing solution (Lonza, ref. CC-5002), and the cells were recovered by centrifugation and counted using a Scepter 2.0 Handheld Automated Cell Counter (Millipore, Billerica, MA, ref. PHCC 20060). For the acinar morphogenesis assay, the RWPE1 and WPE1-NB26 cells were cultured in 3D with KSFM (Life Technologies, ref. 17005-075) supplemented with 50 ng/mL EGF and 2% fetal bovine serum (FBS). The 3D culture was grown in Matrigel (BD Biosciences, San Jose, CA, ref. 356231) according to the top-coat protocol (8). The top-coat assay was preferred to the 3D 'embedded' assay because it requires less time and EHS (Engelbreth–Holm–Swarm Mouse Tumor) and because it facilitates imaging as the colonies are in a single plane (8). Briefly, Matrigel was thawed overnight and poured into 4-well (160 μL of Matrigel, 500 μL of culture media) or 8-well Labtek (90 μL of Matrigel, 250 μL of culture media) plates on ice. For polymerization, Matrigel was incubated for 30 min at 37 °C. Cells were seeded in half the final volume and allowed to adhere for approximately 45 min. The top coat layer containing 8% Matrigel was slowly poured over the attached cells. The culture media was changed every other day. All cells were routinely cultured in a humidified atmosphere with 5% CO_2 at 37 °C. To perform statistical analysis and to determine spheroid-to-acini ratios in the same field of view, a mix of WPE1-NB26 and RWPE1 cells was seeded onto 3D Labtek slide chamber and analyzed. To quantify the effect of TGF beta on acinar formation, we conducted an experiment in which TGF beta was added to RWPE1 3D cell cultures after 3, 5 and 10 days of culture.

After at least 8 days of 3D culture, the cells were fixed with 4% (v/v) paraformaldehyde in PBS for 20 min and washed once with PBS. Actin filaments were stained with TRITC phalloidin (Sigma-Aldrich,

St-Louis, MO, ref. P1951) at a 1:500 dilution for 20 min while nuclei were counterstained with Hoechst (Life Technologies, ref. H-1399) at a 1:7000 dilution. Glass cover slides were mounted on the glass slides with a Dako Fluorescent Mounting Medium kit (Dako, Glostrup, DK, ref. S3023) and stored at 4 °C before imaging.

2.3. Lensfree imaging and microscopy

Our lensfree imaging device is depicted in Fig. 1b. It is based on the technique introduced by Ozcan and Demirci (2008), Seo et al. (2009)). The setup consists of a LED emitting at 610 nm coupled to a 150 μm diameter pinhole and a CMOS image sensor. The characteristics of the three different sensors used during the experiments are detailed in supplementary information S-1. The LED is located 10 cm above the sensor and illuminates the slide chamber that contains the 3D epithelial cell culture. The chamber is put on the CMOS sensor such that the distance between the sensor plane and the cells is approximately 800 μm. An in-line holographic image is then formed on the sensor as a result of the interference between the partially coherent incident light and the light scattered by the cells and/or the acini. Fig. 1a shows the lensfree acquisition of a full chamber of an 8 well Lab-Tek® slide. To image a FOV as large as 9.4 by 7.3 mm^2, we composed a mosaic of 4 24 mm^2 lensfree acquisitions. The acini of interest could then be localized on the lensfree sensor monitoring the full chamber and finely re-analyzed using a fluorescence microscope for comparison. We used the AxioImager Z1 Zeiss microscope equipped with the straight Apotome module for z-stack acquisitions. The microscope was mounted with an AxioCam MRm monochrome digital camera. Optical sectioning of the fluorescent samples was performed to discriminate the 3D structures, i.e., acini with lumen versus spheroids.

3. Results

Our lensfree imaging device was used to image the fully differentiated multicellular assemblies that form acini. Fig. 1 shows the lensfree imaging device and images of a RWPE1 3D cell culture. One can visualize many 3D objects (> 1000) at a glance and look for rare events at the level of single 3D structures. Fig. 1d shows a zoomed-in region of Fig. 1a featuring the lensfree hologram of merged 3D structures, a single 3D object and single epithelial cells. The 3D cultures of epithelial cells are based on the support of cells with a naturally derived soft substrate that comprises a mixture of proteins and growth factors and that allows the homogenous interaction of the cells with their environment in three dimensions.

Successful 3D culture is mostly performed in the presence of Engelbreth–Holm–Swarm (EHS)-derived ECM that directs the induction of glandular epithelial polarity. Secretory epithelia are typically composed of acini (Fig. 2a), a bilayered cellular sphere, and tubules that are cylindrical monolayers forming a network between single acini. The polarity of the acini and the tubules result in the formation of an apical surface facing the lumen and a basolateral surface facing the extracellular matrix. The frequency of acinar formation is expected to be significantly different in RWPE1 and WPE1-NB26 cell lines (Bello-DeOcampo et al., 2001). Indeed, optical confocal sections of DAPI-stained cells after 8 days of growth in Matrigel show that the non-tumorigenic RWPE1 formed acini with well-polarized cells and a distinct lumen (Fig. 2b), whereas WPE1-NB26 cells did not differentiate efficiently and formed many more spheroids (Fig. 2e). The inability to undergo acinar differentiation correlated with their degree of malignancy (Bello-DeOcampo et al., 2001).

By comparing the RWPE1 and WPE1-NB26 3D epithelial cell cultures (Fig. 2) and hence acini (Fig. 2a) and spheroids (Fig. 2b), we observed significant differences between their lensfree holograms. The lensfree holograms of spheroids (Fig. 2f) showed a very bright spot in the middle whereas the holograms of acini with lumens were more uniformly black (Fig. 2c). The difference in gray-level intensity in the center of these two holograms is approximately 100 out of 255 with a background of 5 Gy-levels (Fig. 2i).

We found two other metrics able to discriminate acini with lumen from spheroids, i.e., the Zernike transform and the amplitude holographic reconstruction (see supplementary information S-2). Fig. S-1 shows the analyses based on the Zernike transform comparing the lensfree acquisition of the RWPE1 and WPE1-NB26 3D cell cultures (see supplementary information S-2).

A comparison of Fig. S-1a and f shows that in this experiment, the lensfree holograms of acini and spheroids were not very

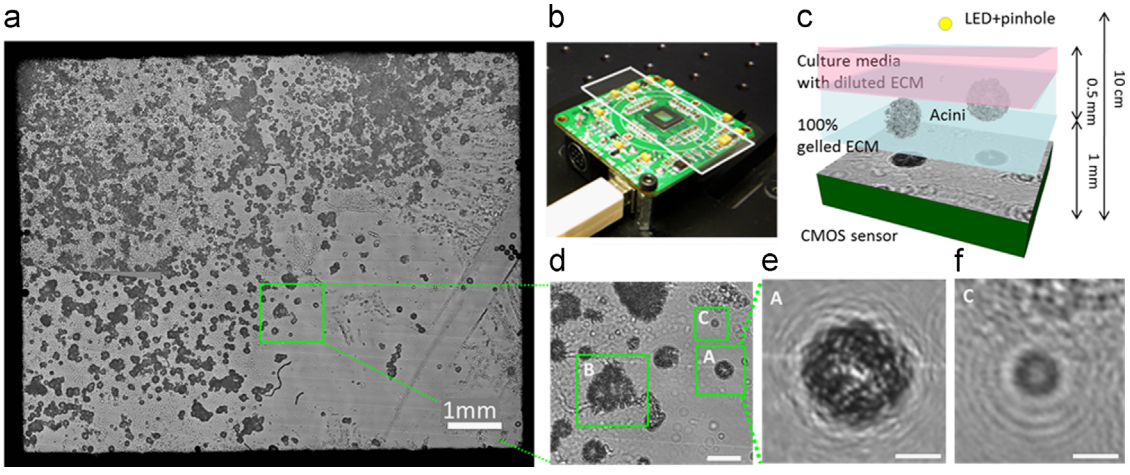

Fig. 1. Lensfree imaging of 3D cultures of epithelial cells. (a) Lensfree imaging of an 8-well Lab-Tek® slide chamber filled with a 3D culture of RWPE1 epithelial cells. Generally, each well contained thousands of acini. To image the entire chamber, we constructed a mosaic of four 24 mm^2 FOV lensfree acquisitions. The CMOS sensor is placed in contact with the chamber slide (b) and allowed to record the lensfree hologram resulting from the interference between the partially coherent incident light and the light scattered by the cells and/or the acini. Illumination is provided by a CMS LED emitting at 610 nm set 10 cm above the chamber. (c) Schematic of the lensfree imaging setup for 3D cultures of epithelial cells (not to scale). Epithelial cells are completely embedded within the extracellular matrix (ECM). (d) The expanded region of the white rectangle in (a) shows the lensfree holograms of (e) an acini (labeled A), merged acini (labeled B) and (f) single cells (labeled C). When the outline of the acini (Fig. 2) is drawn in the lensfree hologram (e), the single cell pattern (f) is much larger than the cell itself. The scale bars are 200 μm and 50 μm in (d) and in (e, f), respectively.

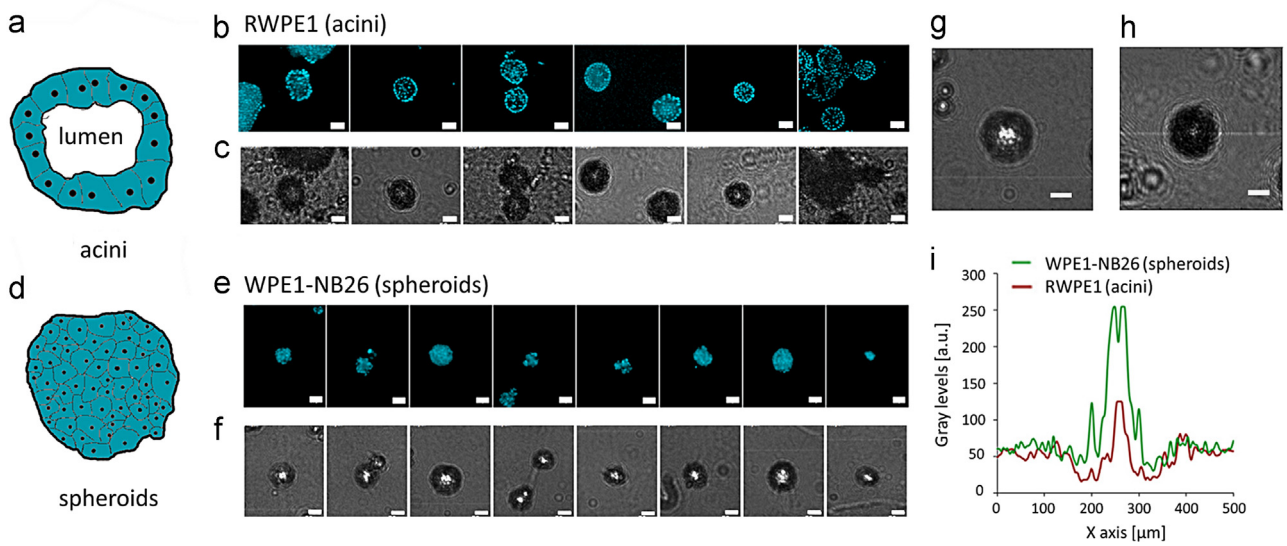

Fig. 2. Lensfree imaging and fluorescence microscopy of acini with lumen versus spheroids. Hoechst-stained 3D cell cultures after 8 days of growth in Matrigel of the (a–b) RWPE-1 and (d–e) WPE1-NB26 cells (20 × magnification, scale bar 50 μm). These acquisitions show the strong difference in acinar formation, i.e., lumen or spheroids. The lensfree holograms of the acini with lumen and the spheroids, whose schematics are depicted in (a) and (d), respectively, present many differences (scale bar 50 μm). At the center of the pattern, the difference in gray-levels yields a value of 100 (onto a full scale of 255). This value is largely above the background noise of our lensfree imaging setup (5 Gy-levels standard deviation) and well above the mean gray levels of 50. Typical lensfree holograms of WPE1-NB26 cells (spheroids) (g) and RWPE-1 cells (acini) (h) scale-bar 50 μm. Intensity profiles measured on lensfree holograms showing the main axis of the WPE1-NB26 cells (spheroids, in green) and the RWPE-1 cells (acini, in red) (i). (For interpretation of the references to color in this figure legend, the reader is referred to the web version of this article.)

different in comparison with Fig. 2. Both the holograms of acini with lumen and spheroids showed a bright spot in the middle and there was less than a one-sigma difference ($N=50$) in the maximum intensity, which made it very difficult to discriminate the two structures. However, by averaging twenty lensfree holograms, we found a subtle halo in those of the acini with lumen (Fig. S-1b) that was not present in the averaged lensfree hologram of the spheroids (Fig. S-1c). To quantify this feature, we implemented a Zernike transform algorithm in ImageJ (Banada et al., 2007; Bae et al., 2012) (see Supplementary information S-2). By calculating the first twenty Zernike moment invariants over a large number of different lensfree holograms of acini (73 RWPE1 objects, 51 WPE1-NB26 objects), we found that three Zernike moments are discriminating, i.e., $|Z_{2,0}|$, $|Z_{4,0}|$ and $|Z_{6,0}|$ (Fig. S-1c, d, e, h, i). In particular, we determined that fixing a threshold to the $|Z_{4,0}|$ Zernike moment allows the measurement of a 1.7σ difference between the RWPE1 and WPE1-NB26 patterns (Fig. S-1j, k).

In some experiments, with a heterogeneous mixture of 3D structures (Fig. 3), the $|Z_{4,0}|$ Zernike moment varied by less than 1σ ($N=50$).

Performing a principal component analysis (PCA) using the first twenty Zernike moment invariants did not improve the discrimination. Where the differences between the acini and spheroids were too small to discriminate with lensfree imaging, we had to consider the 3D structures as 2D objects of which the transmission could be reconstructed by holographic amplitude reconstruction (Fienup, 1982; Soulez et al., 2007) (see Supplementary information). In principle, by applying a threshold to the reconstructed amplitude to detect the spheroids and local maxima to detect all the acini, we thought it is possible to discriminate the acini from the spheroids. To experimentally verify our hypothesis, we performed image reconstruction of the hologram obtained from the plate containing both spheroids and acini. The amplitude reconstruction of RWPE1 and WPE1-NB26 epithelial 3D cell cultures indicated that the percentage of spheroids was 8% ($N=109$) and 60% ($N=181$), respectively (Fig. 3c).

To further investigate the imaging capabilities of our system and to extend our observations, we performed a time course experiment to monitor the dynamic phenotypes induced upon the variation of culture conditions. As little is known about the influence of transforming growth factor on acini formation in a 3D culture of non-malignant prostate cells, we treated epithelial cells at very early stages of 3D culture and induced polarized acini formation with TGF beta-1. We built a dataset of 35 lensfree acquisitions over 9 days, from day 3 to day 12 after TGF beta-1 addition. In total, we acquired and analyzed approximately 10,000 lensfree holograms of single acini and multiacinar structures. Fig. 4 shows the effects of TGF beta-1 on acini size and on the process of multiacinar formation.

There was an inhibition of acinar growth that was dependent on the length of the TGF beta-1 treatment (Fig. 4a). In a control experiment, multiacinar structures predominate and the single acini reach the largest observed size, with a mean diameter of 125 μm and a maximum diameter up to 200 μm. The shorter the TGF beta-1 treatment, the smaller the single acini obtained (Fig. 4b). The mean acini diameter increased by a factor of approximately two in 9 days. Similarly, TGF beta-1 treatment of RWPE1 cells in 3D culture limited the formation of multiacinar structures that predominated in the control experiment. The ratio of the surface covered by multiacinar structures versus single acini was between 5 and 7 in the control experiments, whereas it did not exceed 3 in the presence of TGF beta-1.

Furthermore, we looked at the number of high intensity lensfree holograms (Fig. 5) because they correlated with the structures of spheroids (Fig. 2).

Performing a manual count (ImageJ, cell counter) on four 24 mm^2 lensfree acquisitions of RWPE1 3D cell culture on day 12 of the experiment, we found patterns with strong lensing effects at 34%, 22%, 32% and 13% ($N=1415$) on day 3, 5 and 10 of TGF beta-1 treatment, respectively. No high intensity lensfree holograms were observed with the control wells (Fig. 5g–j). These results are consistent with the measured local maxima distribution (75 Gy-levels noise tolerance, ImageJ). By applying a gray-level threshold at an arbitrary value of 175 (see threshold line in Fig. 5e, f), we found percentages of 26%, 21%, 33% and 16%, which are similar to the data obtained after the manual counting. There was thus a

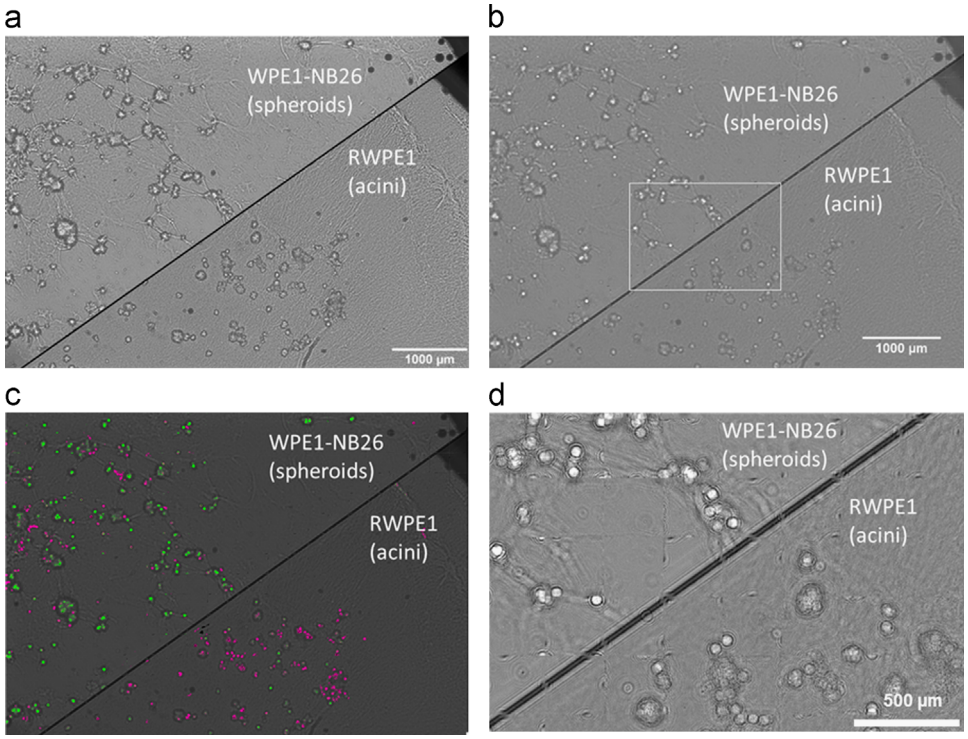

Fig. 3. Holographic reconstruction of acini with lumen versus spheroids. (a) The 24 mm^2 lensfree acquisition of two chambers of an 8-well Labtek® slide containing WPE1-NB26 (top half) and RWPE1 (bottom half) 3D cell cultures. (b) Reconstructed amplitude lensfree images. The white rectangle in (b) is expanded in (d). (c) Local maxima and gray-level thresholding of the reconstructed amplitude lensfree images show the detection of acini with lumen (in purple) and spheroids (in green). (For interpretation of the references to color in this figure legend, the reader is referred to the web version of this article.)

two-fold difference in the number of spheroids between the control and TGF beta-1 experiments.

4. Discussion

The optical observation of biological objects and tissues is traditionally performed using conventional light microscopes and immunofluorescence. However, the quantitative measurement of cellular responses in 3D over periods of time has been hampered (Yue et al., 2012). Therefore, there is a need for alternative microscopy techniques such as label-free, miniaturized and immobilized platforms enabling the study of 3D biological architectures. The lensfree system that we present in this study is a tool to observe epithelial 3D architectures. It does not allow the reconstruction of large 3D features because we did not implement tomography methods (Isikman et al., 2012). Instead, it allows the observation of light propagating through the 3D objects. To correlate these observations with 3D cell structures, we introduced several metrics. Part of our method is the use of appropriate metrics to discriminate spheroids from acini.

We showed that when a lensing effect is observed (Fig. 2), mainly with spheroids, the gray-level threshold could be used to discriminate spheroids from acini. These observations have been confirmed by standard fluorescence techniques. A similar lensing effect acquired by lensfree imaging has been already described (Allier et al., 2010). However, in further experiments, this criterion was not sufficiently discriminating. It is not robust enough to take into account the variations observed in 3D culture experiments arising from the composition and physical properties of the ECM layer that lead to changes in the distance between the object embedded in the ECM and the sensor. Therefore, the gray-level analysis can be used only when the acini are very similar, for example, as micropatterns in standardized 3D cultures (Rodriguez-Fraticelli et al., 2012).

Under more variable conditions, the Zernike transform is preferred to gray-level thresholding. This method is based on the mapping of an image onto a set of polynomials that are perpendicular to each other (see Supporting information S-2). The Zernike moments have been successfully used for the recognition of patterns including the analysis of mammograms (Tahmasbi et al., 2011). The high computational complexity of Zernike moments has often hampered its suitability for real-time applications. Here, we successfully performed discrimination on the basis of only one Zernike moment, i.e., applying simple thresholding, which drastically reduced the computational task. We achieved discrimination between the two populations of acini with two-sigma significance (Fig. S-1). This result is underestimated as it is calculated assuming that all the RWPE1 and WPE1-NB26 cells form acini and spheroids, respectively, which is not the case. Practically, 60–80% of a standard 3D culture of non-malignant epithelial cells forms polarized structures (refs in Yue et al., 2012). Furthermore, we verified that the discrimination is not related to another variable. By measuring the maximum gray level, the mean gray level, the diameter, the kurtosis and the sphericity on different lensfree holograms ($N=120$), we could not find any difference larger than one-sigma between the two populations of acini. This result means that in this experiment, the Zernike transform allowed the identification of different features of the acini with lumen and the spheroids in the lensfree holograms.

A third means of analysis was based on the assumption that the acini can be described as 2D objects whose transmission can be analyzed by holographic reconstruction. Hence, by applying a threshold to the reconstructed amplitude, we successfully estimated the number of acini and spheroids in a culture of RWPE1 and WPE-NB26 cells (Fig. 3).

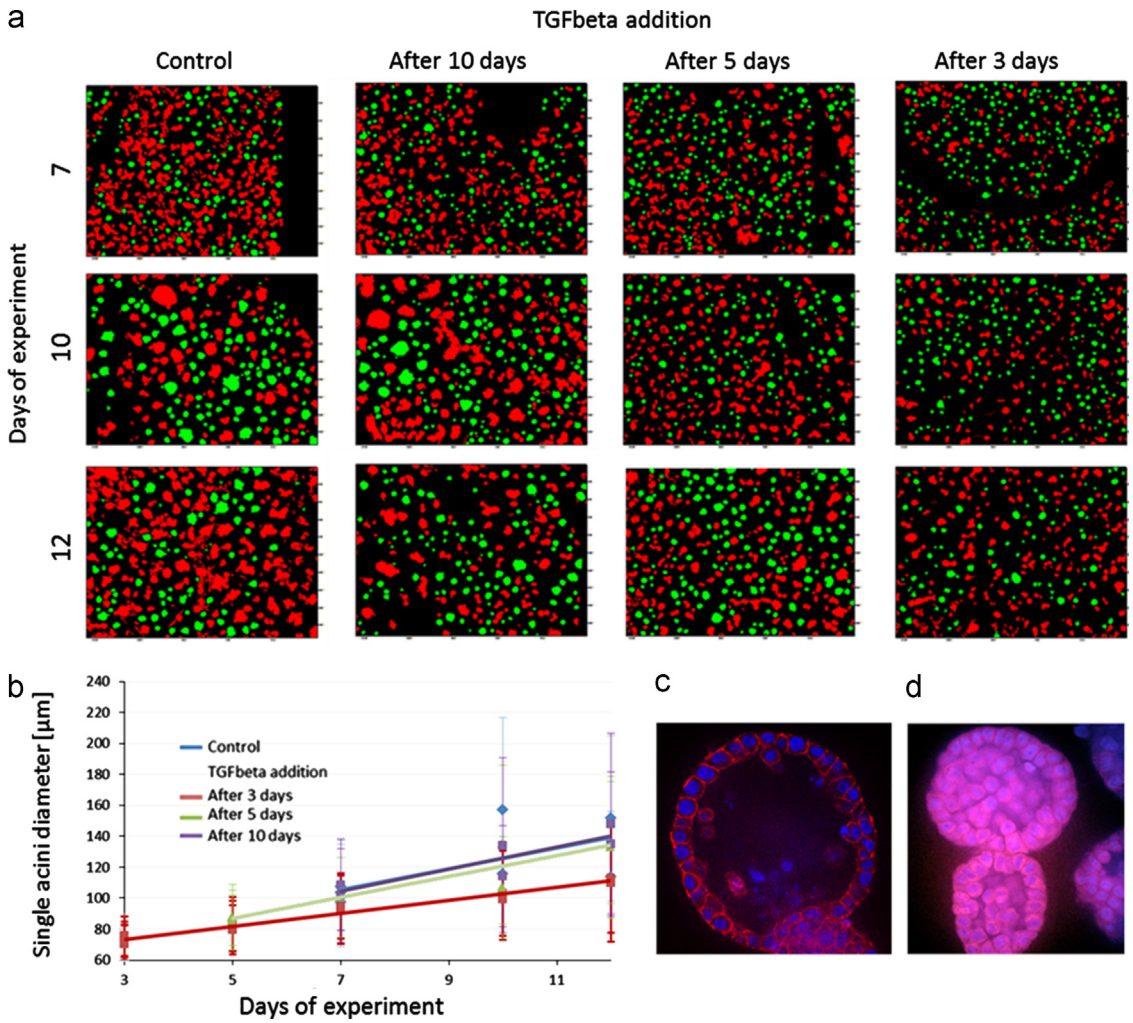

Fig. 4. Influence of TGF beta-1 addition on the acini size and the multiacinar structures. (a) The 24 mm^2 lensfree acquisitions of RWPE1 3D cell cultures 3, 5 and 10 days after TGF beta-1 (3 ng/mL) or no TGF beta-1 addition as a control. Every picture shows the single acini in green and multiacinar structures in red. (b) The mean diameter of each acinus measured from 35 lensfree acquisitions, measured over-time and grouped according to the day of TGF beta-1 addition. The error bars correspond to standard deviations of the diameter measured within one lensfree acquisition ($N=150$). (c, d) RWPE1 cells in 3D culture stained with Hoechst (blue) and phalloidin (red) under control conditions (c) and after 3 days of TGF treatment (d) following 8 days of culture in Matrigel. Notice the reduced diameters of the acini and the presence of cortical actin upon TGF treatment. (For interpretation of the references to color in this figure legend, the reader is referred to the web version of this article.)

The main limitation of those metrics is that the choice for the best metric is experiment-dependent owing to the variability in the optical properties of the acini. There are hidden variables that are inaccessible with our lensfree imaging, e.g., the 3D geometry of the acini, the number of cells, refractivity, absorption and diffusion coefficients, presence and size of the lumen. This caveat explains why we consider these metrics a toolset to be systematically applied to each experiment. If the experiment is performed within a multi-well slide with all necessary control measurements, our approach allows qualitative observations and the counting of the different 3D geometries. At this stage this methodology does not allow the analysis of the properties of every single acinus, to quantify for instance the degree and stage of malignancy. This will be a point of focus for future work.

As a demonstration of our lensfree approach, we have studied the influence of TGF beta-1 (transforming growth factor beta-1) on different acini in 3D cell cultures, and we have monitored over time the polarity status, the acini size and the process of acini merging. TGF beta regulates homeostasis and suppresses tumor progression but little is known about how TGF beta treatment influences the formation of acini in 3D cultures of normal prostate epithelial cells. Our measurements showed that the diameter of each acinus decreased upon TGF beta-1 addition, especially when TGF beta-1 was added at a very early stage of growth (3 days). This in vitro inhibitory growth effect is consistent with the prevention of lumen formation that we observed using two separate metrics (Fig. 5). In contrast, the observed decrease in the number of merging acini was not expected, suggesting that TGF beta-1 could limit signaling between the acini. In control experiments, even at low cell seeding density, the acini were able to migrate and merge with one another. To further monitor their polarity, the ratio between the acini and the spheroids was determined based on the previously obtained gray-level signatures [acini (dark pattern) versus spheroids (bright pattern)]. Unexpectedly, a decrease in the proportion of acini was also observed in the cell populations treated with TGF beta after 10 days in culture, when cells were already well differentiated into acini, which suggests that TGF beta treatment can perturb acinar structure and revert the phenotype. The effect of TGF beta on lumen formation could be mediated by mechanotransduction, given the consistent presence of cortical actin following TGF beta treatment (Fig. 4c–d). Such organization of sub-cortical rings is

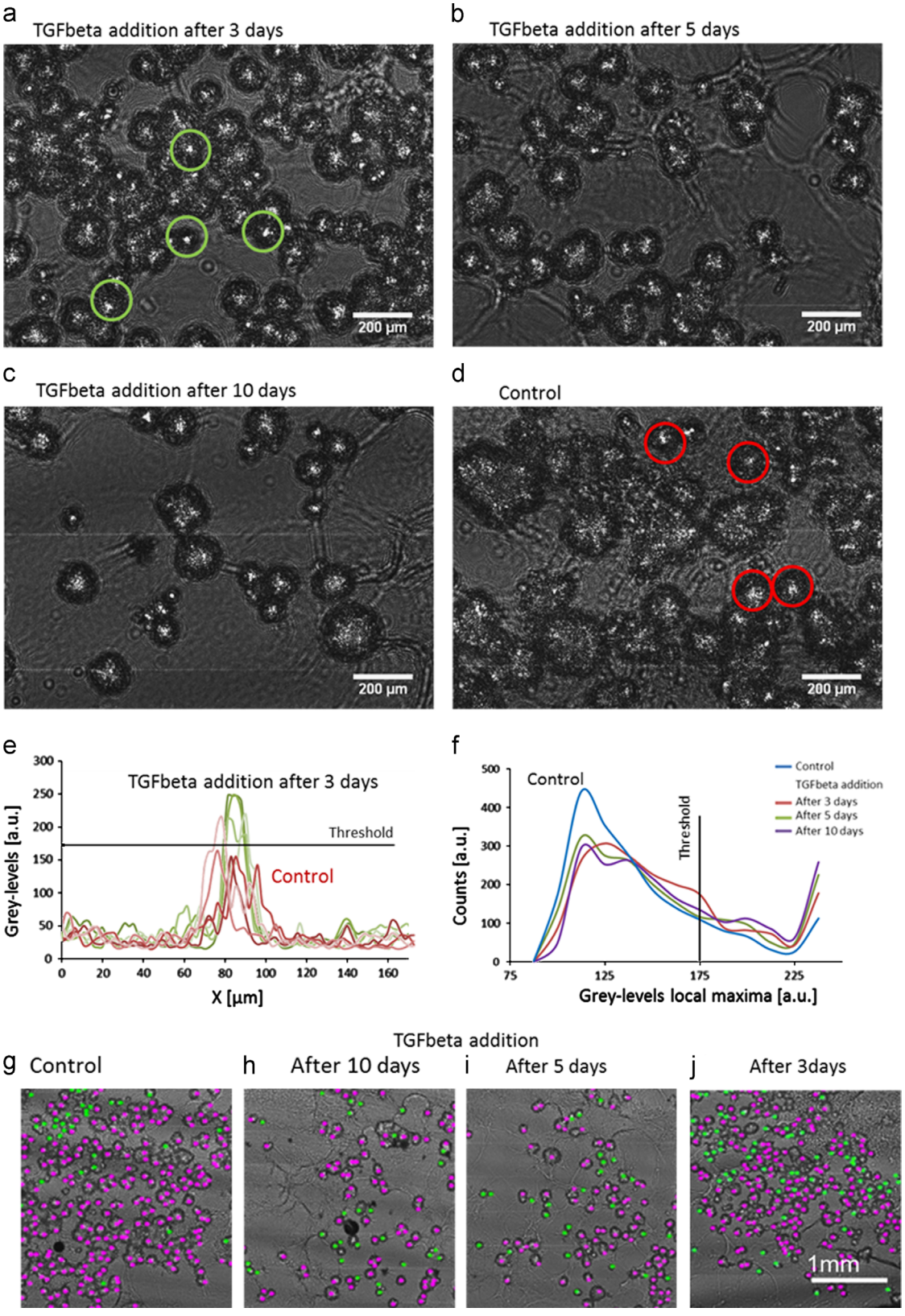

Fig. 5. The influence of TGF beta-1 addition on the number of spheroids. Cropped regions of 24 mm^2 lensfree acquisitions of the RWPE1 3D cell culture on day 12 of the experiment with TGF beta-1 (3 ng/mL) having been added after 3 (a), 5 (b) and 10 days (c) and with no TGF beta-1 treatment serving as a control (d). Note that acini hologram patterns with strong lensing effects are present in the acquisition, showing a very bright spot at the center of each pattern. Intensity profiles of such patterns, with green circles in (a) plotted in green in (e). For comparison, the control acini pattern intensity profiles [red in (d)] are plotted in red in (e). Local maxima distributions measured on four 24 mm^2 lensfree acquisitions (75 Gy-levels noise tolerance, ImageJ) are plotted as a function of the day on which TGF beta-1 had been added. (g, h, i, j) Cropped regions of 24 mm^2 lensfree acquisitions of RWPE1 3D cell cultures on day 12 of experiment as a function of the day on which TGF beta-1 had been added. Lensfree holograms of strongly lensing acini are marked as green points after manual counting (cell counter, ImageJ). Single acini and multiacinar structure are marked as purple points. (For interpretation of the references to color in this figure legend, the reader is referred to the web version of this article.)

known to be associated with cell tension that could mediate TGF beta activation (Giacomini et al., 2012). Interestingly, the cortical actin was still present after 9 days of treatment, indicating the long-term effects of TGF beta.

When combined with 3D culture and the appropriate metrics, our lensfree system allows the discrimination of polarized assemblies (acini) from non-polarized architectures (spheroids). As the maintenance of polarity is critical for the function of epithelial cells, our system provides a relevant tool to decipher biological processes in development and morphogenesis in a more physiological context than in traditional 2D cultures. Biomedical and drug screening applications are detailed in Supplementary information S-3.

5. Conclusions

This study demonstrates for the first time that lensfree imaging is a new methodology able to analyze distinct 3D cellular objects and discriminate acini from spheroids. It could be extensively used for studying cell–cell and cell–environment interactions by modulating the biochemical and mechanical stimuli within the ECM. We believe that this technique will be a powerful method for the future large field analysis of multiple soluble effects, including fundamental and pharmacological research in carcinogenesis.

Acknowledgments

The work at CEA-Leti was supported by the Carnot Institutes Network.

Appendix A. Supporting information

Supplementary data associated with this article can be found in the online version at http://dx.doi.org/10.1016/j.bios.2013.05.001.

References

Allier, C.P., Hiernard, G., Poher, V., Dinten, J.M., 2010. Biomedical Optics Express 1 (3), 762–770.
Bae, E., Ying, D., Kramer, D., Patsekin, V., Rajwa, B., Holdman, C., Sturgis, J., Davisson, V.J., Robinson, P., 2012. Journal of Biological Engineering 6 (1), 12.
Banada, P.P., Guo, S., Bayraktar, B., Bae, E., Rajwa, B., Robinson, J.P., Hirleman, E.D., Bhunia, A.K., 2007. Biosensors and Bioelectronics 22 (8), 1664–1671.
Baum, C., Dullmann., J., Li, Z., Fehse, B., Meyer, J., Williams, D.A., von Kalle, C., 2003. Blood 101 (6), 2099–2114.
Bello-DeOcampo, D., Kleinman, H.K., Webber, M.M., 2001. Mutation Research 480–481, 209–217.
Bishara, W., Sikora, U., Mudanyali, O., Su, T-W., Yaglidere, O., et al., 2011. Lab on a Chip 11 (7), 1276–1279.
Bryant, D.M., Mostov, K.E., 2008. Nature Reviews Molecular Cell Biology 9 (11), 887–901.
Debnath, J., Brugge, J.S., 2005. Nature Reviews Cancer 5 (9), 675–688.
Fienup, J.R., 1982. Applied Optics 21 (15), 2758–2769.
Giacomini, M.M., Travis, M.A., Kudo, M., Sheppard, D., 2012. Experimental Cell Research 318, 716–722.
Greenbaum, A., Luo, W., Su, T.W., Göröcs, Z., Xue, L., Isikman, S.O., Coskun, A.F., Mudanyali, O., Ozcan, A., 2012. Nature Methods 9, 889–895.
Hebner, C., Weaver, V.M., Debnath, J., 2008. Annual Review of Pathology 3, 313–339.
Isikman, S.O., Bishara, W., Mavandadi, S., Yu, F.W., Feng, S., Lau, R., Ozcan, A., et al., 2011. Proceedings of the National Academy of Sciences of USA 108 (18), 7296–7301.
Isikman, S.O., Bishara, W., Mudanyali, O., Sencan, I., Ting-Wei, Su., Tseng, D.K., 2012. IEEE Journal of Selected Topics in Quantum Electronics 18 (3), 1059–1072.
Lee, G.Y., Kenny, P.A, Lee, E.H., Bissell, M.J., 2007. Nature Methods 4 (4), 359–365.
Mailleux, A.A., Overholtzer, M., Brugge, J.S., 2008. Cell Cycle 7 (1), 57–62.
Moscelli, N., Van den Driesche, S., Witarski, W., Pastorekova, S., Vellekoop, M.J., 2011. Sensors and Actuators A: Physical 172 (1), 175–180.
Mudanyali, O., Bishara, W., Ozcan, A., 2011. Optics Express 19 (18), 17378–17389.
Mudanyali, O, McLeod, E, Luo, W, et al., 2013. Nature Photonics 7, 247–254.
O'Brien, L.E., Zegers, M.M.P., Mostov, K.E., 2002. Nature Reviews 3, 531–537.
Ozcan, A., Demirci, U., 2008. Lab on Chips 8 (1), 98–106.
Pampaloni, F., Reynaud, E.G., Stelzer, E.H., 2007. Nature Reviews Molecular Cell Biology 8 (10), 839–845.
Pearson, J.F., Hughes, S., Chambers, K., Lang, S.H., 2009. Cell Death and Differentiation 16 (3), 475–482.
Rodriguez-Fraticelli, A.E., Auzan, M., Alonso, M.A., Bornens, M., Martin-Belmonte, F., 2012. Journal of Cell Biology 198 (6), 1011–1023.
Seo, S., Su, T.W., Tseng, D.K., Erlinger, A., Ozcan, A., 2009. Lab on Chips 9 (6), 777–787.
Soulez, F., Denis, L., Fournier, C., Thiebaut, E., Goepfert, C., 2007. Journal of the Optical Society of America A: Optics, Image and Vision 24 (4), 1164–1171.
Su, T.W., Xue, L., Ozcan, A., 2012. Proceedings of the National Academy of Sciences of USA 109 (40), 16018–16022.
Tahmasbi, A., Saki, F., Shoukouhi, S.B., 2011. Computers in Biology and Medicine 41, 726–735.
Weidling, J., Isikman, S.O., Greenbaum, A., Ozcan, A., Botvinick, E., 2012. Journal of Biomedical Optics 17 (12) 126018.
Yue, S., Cardenas-Mora, J.M., Chaboub, L.S., Lelièvre, S.A., Cheng, J-X., 2012. Biophysical Journal 102, 1215–1223.
Zegers, M.M., O'Brien, L.E., Yu, W., Datta, A., Mostov, K.E., 2003. Trends in Cell Biology 13 (4), 169–176.
Zheng, G., Lee, S.A., Antebi, Y., Elowitz, M.B., Yang, C., 2011. Proceedings of the National Academy of Sciences of USA 108 (41), 16889–16894.